Harmonic content of electron-impact source functions in inductively coupled plasmas using an "on-the-fly" Monte Carlo technique

Arvind Sankaran[a] and Mark J. Kushner[b]
University of Illinois, 1406 W. Green St., Urbana, Illinois 61801

(Received 4 February 2002; accepted for publication 24 April 2002)

Electron temperatures in low-pressure (<10s mTorr) inductively coupled plasma (ICP) reactors operating at 10s MHz do not significantly vary during the radio frequency (rf) cycle. There can be, however, considerable modulation of electron-impact source functions having high-threshold energies due to modulation of the tail of the electron energy distributions (EEDs). In many instances, it is convenient to use cycle-averaged values for these quantities in models due to the computational burden of computing and storing spatial and time-dependent EEDs. In this paper an "on-the-fly" (OTF) Monte Carlo technique is described to address these time-dependent plasma parameters. The OTF method directly computes moments of the EEDs during advancement of the trajectories of the pseudoparticles, thereby reducing computational complexities. The method can also be used to directly calculate the harmonic components of excitation, which can subsequently be used to reconstruct the time-dependent source functions. The OTF technique was incorporated into a two-dimensional plasma equipment model to investigate the time dependence of electron-impact source functions in low-pressure ICP systems. We found that even harmonics dominated the source functions for high-threshold processes, and that the harmonic content decreased with increasing frequency and increased with increasing pressure. We also observed axial pulses of excitation and increasing harmonic content at low pressures which are attributed to nonlinear Lorentz force acceleration and nonlocal transport. © *2002 American Institute of Physics.*
[DOI: 10.1063/1.1487455]

I. INTRODUCTION

The trend in plasma processing as used for microelectronics fabrication is towards systems operating at lower pressures (<10s mTorr).[1] Inductively coupled plasma (ICP) reactors operating at these pressures are typically thought of as providing a continuous wave (cw) source of excitation.[2–6] This is a good approximation for properties which largely depend on the average electron energy or temperature whose value is typically considered constant during the radio frequency (rf) cycle.[7] As a consequence, multidimensional models for ICP reactors have traditionally used temperatures or electron energy distributions (EEDs) averaged over the rf cycles to determine rate coefficients and source functions for electron-impact processes.[2,4,5] Although the electron temperatures in low-pressure ICPs, a quantity dependent on the bulk of the EED, may not significantly vary during the rf cycle, the tail of the EED may, in fact, have phase-dependent properties.[8–11] As a result, rate coefficients and source functions for electron-impact reactions having high-threshold energies may have a phase dependence.[8,10]

The phase dependence of electron-impact processes in rf excited systems has been extensively previously investigated in the context of capacitively coupled discharges (CCPs).[12–16] These systems, in addition to having excitation which is dominated by sheath heating, typically operate at higher pressures (100s mTorr). As the rate of equilibration of EEDs with the excitation source scales with the collision frequency, source functions in CCPs operating at higher pressures would be expected to exhibit more harmonic behavior than ICPs operating at lower pressure. For example, Graves developed a hybrid model for rf excited CCPs in which solutions were expanded in a Fourier series in time and linear finite element basis functions in space.[12] He found significant modulation in space and time in rates of ionization and excitation. Sommerer *et al.* investigated a similar CCP system having an interelectrode spacing of 4 cm operating in 100 mTorr helium at 13.56 MHz.[13] The ionization rates were found to peak near the sheath-bulk boundary during the cathodic phase while the expanding sheath accelerates the electrons that had migrated toward the electrode during the anodic cycle. The difference in collisionality between the bulk and tail electrons explained phase differences in excitation rates produced by low- and high-energy electrons. Meyyappan and Govindan also investigated time-dependent excitation in one-dimensional CCP reactors.[8,14] They found, for example, that in argon at 100s mTorr, ionization rates had maxima twice a cycle with a location which propagated into the plasma with speeds of $\approx 5\times 10^7$ cm/s. Surendra *et al.* referred to this phenomenon as a moving ionization "pulse."[15] Petrovic *et al.*[16] measured optical emission from CCPs sustained in SF_6/N_2 at frequencies of 20 kHz to 20 MHz at pressures of 0.05–1 Torr. They observed similar spatially dependent harmonic emission with propagation speeds of 3×10^6 cm/s.

[a]Department of Chemical Engineering; electronic mail: asankara@uiuc.edu
[b]Department of Electrical and Computer Engineering; electronic mail: mjk@uiuc.edu

The harmonic content discussed in these previous investigations results from, to a large degree, linear processes. These processes are periodic accelerations of electrons by electrostatic fields by either oscillating sheaths resulting in stochastic (collisionless) heating or oscillating electric fields in the bulk plasma producing collisional heating. In lower pressure, electromagnetically driven devices, such as ICPs, the opportunity presents itself for both these linear mechanisms and for nonlinear processes, in particular $\vec{v}\times\vec{B}$ Lorentz forces (F_L). These accelerations result from electrons having an azimuthal component of velocity produced by the azimuthal inductively coupled electric field (force F_E) and the dominantly radial rf magnetic field combining to produce an axial acceleration having a second-harmonic component.[11,17,18] (These effects have also been investigated in the context of pondermotive forces.[19,20]) For example, Godyak has found that F_L/F_E can exceed unity at frequencies of a few megahertz (where the rf magnetic field is larger) and pressures lower than 10 mTorr (where collisional mixing of velocity components is less important). The strong axial force may, in fact, be sufficiently large to deplete low-energy electrons in the skin layer and so produce an electrostatic potential.[11] These effects can be measured as a second harmonic component in the plasma potential.[18] The second-harmonic component of the nonlinear Lorentz force (NLF) scales as $1/(\omega\nu_m)$, where ν_m is the total electron momentum transfer collision frequency (including elastic and inelastic processes) and ω is the fundamental driving frequency of the electromagnetic field.[21]

Recent investigations of phase resolved emission from ICPs sustained on Ar and O_2 at pressures of 15–300 mTorr have also shown significant harmonic content. Tadokoro *et al.*[8] made tomographic measurements of emission from $Ar(3p_5)$ (radiative lifetime 90 ns) and $O(3p^3P)$ (radiative lifetime 34 ns) at 13.56 MHz in a cylindrically symmetric ICP. The scaling of the harmonic content for the Ar plasmas (decreasing with increasing pressure) was different from that for the oxygen discharges (increasing with increasing pressure). Tadokoro *et al.* suggest that $\vec{E}\times\vec{B}$ drift, produced by the quasi-dc radial electrostatic field and the axial rf magnetic field, produced periodic accelerations in the azimuthal direction.

The purpose of the work reported here was to investigate the time dependence of excitation rates in low pressure, ICP systems. Our specific interest was the time-harmonic content of these rates and their two-dimensional spatial dependence. This latter behavior should provide insight to noncollisional electron transport and NLF. In order to capture the dynamics of the EEDs, a kinetic Monte Carlo (MC) simulation was used as the electron transport module of a plasma equipment model. In doing so, a MC technique called ''on-the-fly'' (OTF) was developed wherein statistics are collected for the harmonic content of moments of the EED as opposed to collecting statistics on the time dependence of the EED itself. The model and the OTF technique are described in Sec. II. The model was used to investigate ICPs sustained in Ar/N_2 gas mixtures while varying excitation frequency, pressure, and mole fraction of N_2 and those results are discussed in Sec. III. We found that similar to CCP systems, the rates of high-threshold processes such as ionization had significant harmonic content, whereas low-threshold processes, such as vibrational excitation, were well represented by time averaged values.

II. DESCRIPTION OF MODEL

The OTF method, developed to investigate harmonics of excitation in ICPs, was implemented into a two-dimensional simulator, the Hybrid Plasma Equipment Model (HPEM). The HPEM will first be briefly described followed by a description of the OTF method. The HPEM is a modular designed to numerically investigate low-pressure and low-temperature plasma processing reactors in two dimensions; and is described in detail in Refs. 22, 23, and references listed therein. The main modules are the electromagnetics module (EMM), electron energy transport module (EETM), and the fluid kinetics module (FKM). The HPEM iterates on these coupled modules to generate a cycle-to-cycle quasi-steady state. Inductively coupled electromagnetic fields are computed in the EMM. These fields are used in the EETM to generate electron-transport coefficients and electron-impact source functions. These values are produced as a function of position by using either the electron Monte Carlo simulation (EMCS) or by solving the electron energy equation coupled with a solution of Boltzmann's equation obtained using a two-term spherical harmonic expansion. (In this paper, the EMCS is employed.) The transport coefficients and source functions are transferred to the FKM which solves separate fluid continuity, momentum, and energy equations for all neutral and ion species, while coupling a semi-implicit solution of Poisson's equation for the electric potential with a drift-diffusion formulation for the electron density. The densities, conductivity, and the time-dependent electrostatic fields obtained from the FKM are then transferred to the EMM and EETM. The modules are iterated until a converged solution is obtained.

The specifics of the algorithms employed in the EMCS have recently been described in detail in Ref. 23 and so will be only briefly summarized here. Electron pseudoparticles are initially distributed in the reactor with a spatial distribution provided by the electron density computed in the FKM. The trajectories of the pseudoparticles are advanced using the electromagnetic fields from the EMM and the electrostatic fields from the FKM.

$$\frac{d\vec{r}}{dt}=\vec{v},\quad \frac{d\vec{v}}{dt}=\frac{q_e}{m_e}(\vec{E}+\vec{v}\times\vec{B}), \tag{1}$$

where $\vec{v}$, $\vec{E}$, and $\vec{B}$ are the electron velocity, local electric field, and magnetic field, respectively. $\vec{E}$ contains contributions from the inductively coupled electric field from the EMM and the electrostatic field from the FKM. In the absence of an externally applied magnetostatic field, $\vec{B}$ contains contributions from only the electromagnetic field. Time steps are chosen to be less than 0.01 of the rf period, 0.01 of the local electron cyclotron frequency, the time to cross half the local computational cell or the time to the next collision, whichever is smaller. The integration scheme is a second-order predictor-corrector method. Several hundred to a few

thousand particles are integrated in time for 10–100 s rf cycles each iteration through the HPEM. Statistics on the location and energy of each particle are recorded with every update of a pseudoparticle's trajectory using finite-sized particle (FSP) techniques.[24] The statistics are weighted by the time step used for the integrating the trajectory.

Collisions are included with anisotropic scattering, incorporating null collision cross sections to account for energy and spatial dependencies in the collision frequencies. For purposes of collecting statistics, the electron energy range is divided into discrete energy bins with widths which are generally smaller at lower energies to resolve more complex collision cross sections, and larger at higher energies where cross sections tend to be smoother. The total collision frequency ν_i within energy bin i is computed by summing all possible collisions within the energy range

$$\nu_i=\left(\frac{2\varepsilon_i}{m_e}\right)^{1/2}\sum_{j,k}\ \sigma_{ijk}N_j\,, \tag{2}$$

where ε_i is the average energy within the bin, σ_{ijk} is the cross section at energy i, for species j and collision process k, and N_j is the number density of species j. The time between the collisions is randomly determined using the maximum collision frequency for the energy range of interest, $\Delta t = -1/\nu \ln(r)$, $r=(0,1)$. At the time of a collision, the reaction that occurs is randomly chosen from all the possible processes for that energy bin. The velocity of the electrons is adjusted based on the type of collision it undergoes. If the collision is null then the electron's trajectory is left unaltered.

The statistics for computing spatially dependent, time-averaged EEDs are updated with each move of a pseudoparticle. The update of the raw statistics F_{il} for energy bin i and mesh point l is

$$F_{il}\rightarrow F_{il}+\sum_j\ w_j\delta\left[\left(\varepsilon_i\pm\frac{1}{2}\Delta\varepsilon_i\right)-\varepsilon_j\right]\cdot\sum_k\ \alpha_k\delta\left[\left(\vec{r}_{l+k}\pm\frac{1}{2}\Delta\vec{r}_{l+k}\right)-\vec{r}_j\right], \tag{3}$$

where the summation is over particles j, w_j is the weighting of the particle, ε_j is its energy, $\Delta\varepsilon_i$ is the width of the energy bin, $\vec{r}_j$ is the location of the particle, and $\Delta\vec{r}_i$ is the width of the mesh cell. The weighting w_j is a product of at least two factors; the relative number of electrons each pseudoparticle represents and the time step used to advance the trajectory. α_k is spatial weighting for the particle's and neighboring cells to distribute the particle's contribution according to FSP principles. The EEDs f_{il} are obtained from the raw statistics F_{il} by requiring the normalization constant A_l at each spatial location to yield

$$A_l\sum_i\ F_{il}=\sum_i\ f_{il}\varepsilon_i^{1/2}\Delta\varepsilon_i=1. \tag{4}$$

Given the f_{il} at the end of the EMCS, the electron temperature, collision frequency and electron-impact rate coefficients are computed as a function of position. (The electron temperature is defined by convention to be $T_e=2/3\ \langle\varepsilon\rangle$.) The electron impact rate coefficient (k_{ml}) for electron-impact process m and location l is then obtained from

$$k_{ml}=\int_0^\infty\left(\frac{2\varepsilon}{m_e}\right)^{1/2}\sigma_m(\varepsilon)f_l(\varepsilon)\varepsilon^{1/2}d\varepsilon=\sum_i\ \left(\frac{2\varepsilon_i}{m_e}\right)^{1/2}\sigma_{mi}f_{il}\varepsilon_i^{1/2}\Delta\varepsilon_i \tag{5}$$

or equivalently,

$$k_{ml}=\frac{\Sigma_i F_{il}v_i\sigma_{mi}}{\Sigma_i F_{il}}, \tag{6}$$

where v_i is the electron speed.

This method of producing rate coefficients or source functions produces spatially dependent but time-averaged values. To obtain time-dependent values, F_{il} would need to be additionally binned by phase in the rf cycle. In doing so, there are implications with respect to memory requirements and computational burden to obtain acceptable statistics, particularly for three-dimensional applications. To address these issues, a method of sampling particles was developed in which one needs to calculate only moments of the distribution function and this is done ''on-the-fly'' (OTF). As a result, in contrast to the conventional Monte Carlo method, the time-dependent distribution functions are not calculated explicitly and thus are not stored either. The basic algorithms just described for the conventional EMCS are retained. Only the method of collecting statistics is different.

In the OTF method the collection of raw statistics F_{il} is replaced by a continuing summation whose asymptotic value in time produces the k_{ml} described by Eq. (6). That is, at time step s, we compute

$$\Delta k_{ml}^s=\sum_j\ w_j\sigma_m(\varepsilon_j)v_j\sum_k\ \delta\left[\left(\vec{r}_{l+k}\pm\frac{1}{2}\Delta\vec{r}_{l+k}\right)-\vec{r}_j\right], \tag{7a}$$

$$\Delta w_l^s=\sum_j\ w_j\sum_k\ \delta\left[\left(\vec{r}_{l+k}\pm\frac{1}{2}\Delta\vec{r}_{l+k}\right)-\vec{r}_j\right], \tag{7b}$$

where Δk_{ml}^s and Δw_l^s are the incremental updates to the rate coefficient and total weighting. The rate coefficient for process m at time s is then obtained from

$$k_{ml}^s=\frac{k_{ml}^{s-1}w_{ml}^{s-1}+\Delta k_{ml}^s}{w_l^s}\text{ where }\ w_l^s=w_l^{s-1}+\Delta w_l^s\,. \tag{8}$$

At any given instant during the EMCS, values for the rate coefficients are immediately available based on the statistics taken to date. Although continuously updating the rate coefficients in this manner is not absolutely critical to obtaining the time-dependent values discussed later, it is convenient in that the rate coefficients are available at any time for use, for example, by another processor during a computationally parallel implementation of the model. As time progresses and more statistics are gathered, k_{ml} simply becomes more accurate. The OTF method has potential advantages over the conventional EMCS by being more accurate than calculating and storing intermediate values of the EED followed by calculating the rate coefficients. Although the OTF bins par-

ticles in space, it avoids discretization or the binning of the electrons in energy and time, and so can utilize the full continuum nature of the EED. The method is advantageous from a computational standpoint as well. Since moments of the distribution function are less sensitive to statistical noise than the EED itself, fewer particles are required in the simulation.

One of the features of the OTF technique is the ability to additionally calculate the Fourier components of the electron-transport coefficients. From these components, one can then reconstruct the time dependence of electron-impact reactions. To calculate these Fourier components the corresponding harmonic terms are incorporated into Eq. (7). (The fundamental frequency ω is taken to be the driving frequency of the antenna.) For example the Fourier component for the n-th harmonic at frequency $n\omega$ is obtained by replacing Eq. (7a) with

$$\Delta k^s_{nml} = \sum_j w_j \sigma_m(\varepsilon_j) v_j \exp(in\omega t_j) \times \sum_k \delta\left[\left(\vec{r}_{l+k} \pm \frac{1}{2}\Delta\vec{r}_{l+k}\right) - \vec{r}_j\right]. \quad (9)$$

The normalization factor is obtained in the same fashion as in Eq. (7b). This procedure produces a complex rate coefficient. The amplitude S^I_{nml} and phase ϕ^I_{nml} of the source function for the n-th harmonic for the I-th iteration through the EMCS is then obtained from

$$S^I_{nml} = [e]_{I-1}|k_{nml}|N_{I-1,l}, \quad \phi^I_{nml} = \tan^{-1}\frac{\mathrm{Im}(k_{nml})}{\mathrm{Re}(k_{nml})}, \quad (10)$$

where $[e]_{I-1,l}$ and $N_{I-1,l}$ are the electron density and density of the gas collision partner at the end of the previous iteration. The time-dependent electron impact source functions used in the continuity equations for plasma species in the current iteration are then

$$S^I_{ml}(t) = \max\left[0, \sum_{n=0}^{n_m} S^I_{nml}\sin(n\omega t + \phi^I_{nml})\right], \quad (11)$$

where n_m is the number of harmonics computed. The source function for any given electron-impact event should always be positive. The maximum function in Eq. (11) is used to account for noise in the EMCS which might result in the sum of the phase weighted amplitudes being negative.

The classic definition of skin depth is for a plasma in which there are no sources of ionization. Although those conditions do not strictly apply here, we nevertheless use the terminology skin depth (or skin layer) to denote the distance in the amplitude of the electric field decays by $1/e$.[25]

For validation purposes, results from the HPEM using the conventional Monte Carlo method and the OTF technique were compared for an ICP reactor using a 5 mTorr $Ar/N_2 = 90/10$ gas mixture. The reactor has a four-turn flat antenna and a 6-cm substrate to window gap, as shown in Fig. 1. Gas is injected through a shower head nozzle and pumped annularly from around the substrate. The final reactor averaged gas temperature was 415 K for a power deposition of 650 W at 13.56 MHz. (These are the ''base case'' operating conditions.) The resulting time-averaged electron densities and time-averaged source functions for electron-impact ionization of argon are shown in Fig. 1. (The source function for ionization is $[e]k_I[\mathrm{Ar}]$ where k_I is the rate coefficient for direct electron-impact ionization of the ground state.) The spatial distributions and magnitudes of the electron densities are essentially the same for the conventional MC and OTF methods, with the OTF providing a few percent higher density, resulting from a few percent higher source function. The spatial distribution of the source function has small differences at small values, largely a result of this statistical noise. Due to the more collisional nature of the Ar/N_2 gas mixture compared to only argon, the electron-density peaks in the vicinity of the maximum in the source function, as opposed to the pure Ar case which, for otherwise similar operating conditions, would have an on-axis peak. T_e is also more peaked in the region of largest power deposition (under the coils) compared to the pure Ar case where the electron temperature has less severe gradients. The presence of N_2 reduces both the energy relaxation distance (due to excitation of the low-lying vibrational and rotational states) and reduces the electron thermal conductivity, thereby restricting the peak in electron temperature.

III. HARMONIC CONTENT OF SOURCE FUNCTIONS

In this section, the harmonic content of electron-impact source functions produced in ICPs sustained in Ar/N_2 gas mixtures will be discussed. The rational for this choice of gases is that vibrational excitation of N_2 has low-threshold energies (<1 eV) and is produced in large part by the bulk of the EED. Electron-impact processes with Ar, particularly ionization, are high-threshold reactions and hence are sensitive to the tail of the EED. We can expect two classes of harmonic behavior, both of which are likely to have an even harmonic component. The first dominantly results from collisional heating by the azimuthal electric field, E_θ. The spatial location of this harmonic excitation should be where the E_θ is largest, in the skin layer. Since acceleration is azimuthal (in this case, parallel to the top dielectric), even non-collisional heating may not stray far from the skin layer. The modulation of the EEDs in this manner, is dependent on the rf frequency and the energy-dependent collision frequency, and generally scales as ν_m/ω. The tail of the EED, usually being more collisional than the bulk (in this case, by a factor of two or more), is expected to be more modulated than the bulk distribution in the limit that heating is collisional, and so high-threshold processes should have more modulation. The second source of modulation results from NLF. Its signature is that NLF acceleration will be dominantly in the axial direction with a second-harmonic component.

As diagnostics for the differences between bulk and tail behavior, we will examine electron source functions for vibrational excitation of $N_2(v=1)$ with threshold energy $\Delta\varepsilon = 0.29$ eV, and ionization of Ar with threshold $\Delta\varepsilon = 16$ eV. The approximate trends for expected behavior may be predicted by the scalings shown in Fig. 2. Here, the total momentum-transfer collision frequencies (elastic and inelastic) for the bulk and tail of the EED are plotted as a function

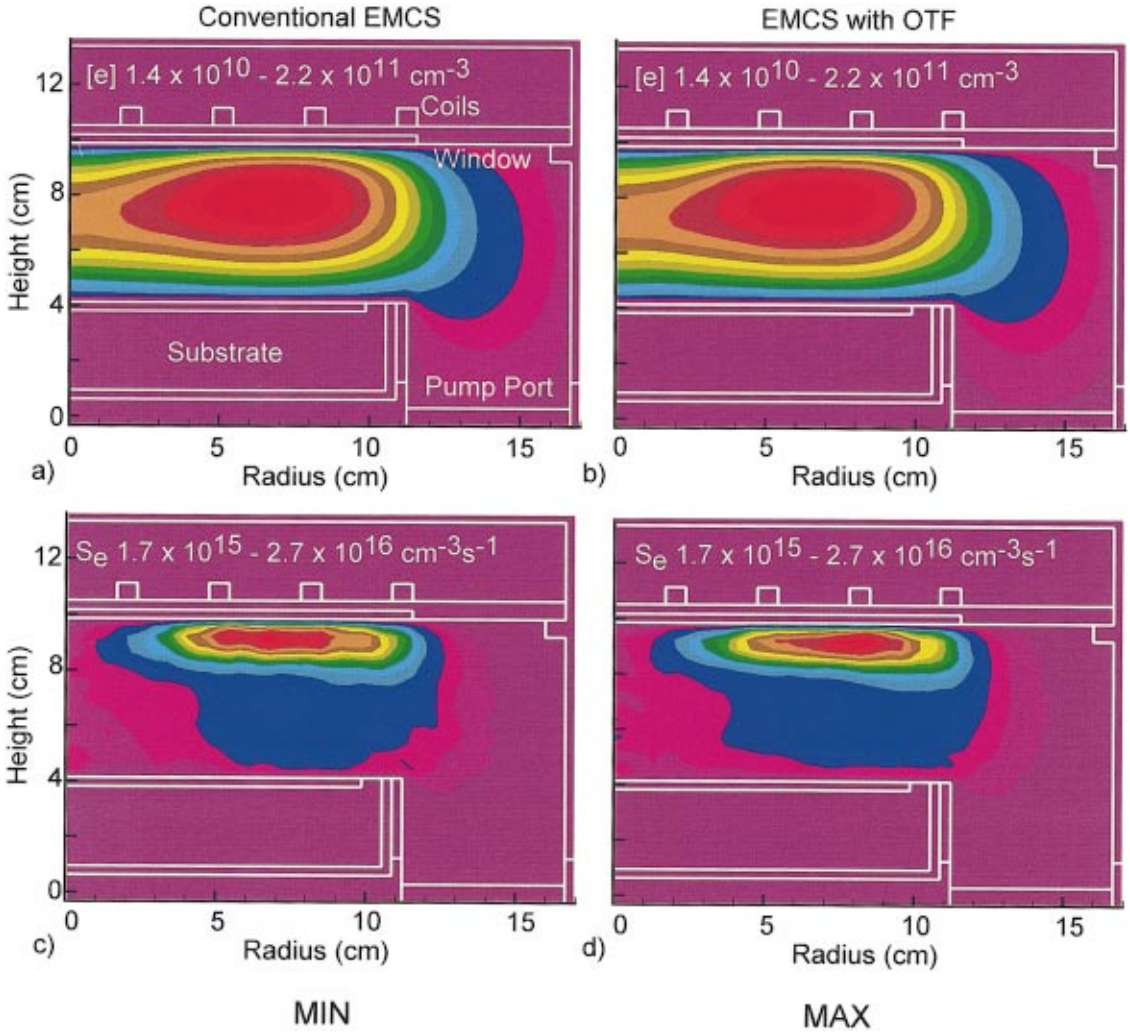

FIG. 1. (Color) Time-averaged electron density in an ICP reactor obtained using (a) conventional MCS method and (b) OTF method; and time-averaged source functions for electron-impact ionization of ground-state argon using (c) conventional MCS method and (d) OTF method. Operating conditions are $Ar/N_2=90/10$, 5 mTorr, 13.56 MHz, and power deposition of 650 W.

of average energy for $Ar/N_2=90/10$. These results were obtained by solving the zero-dimensional, time-independent Boltzmann's equation using a two-term spherical harmonic expansion while varying the electric field/gas number density (E/N). The tail of the EED was arbitrarily defined as containing those electrons having energies greater than twice the average energy. Over the range of expected average energies (4–6 eV), the collision frequency of electrons in the tail of the EED is significantly larger than that in the bulk. This higher-collision frequency also translates into a shorter mean free path. For rf frequencies of a few megahertz both the tail and the bulk are sufficiently collisional that both segments of the EED should have modulation. For rf frequencies of 10s MHz, it is likely that only the tail will be modulated. The second parameter in Fig. 2 is $\nu_\varepsilon=(1/\varepsilon)(d\varepsilon/dt)$, the characteristic frequency at which electrons of a given energy lose that energy. At low-average energies, the division between the bulk and the tail of the EED sweeps across the vibrational excitation cross sections of N_2, resulting in nonmonotonic behavior for ν_ε. At higher-average energies, it is again the tail electrons which lose their energy at a higher rate, and so would be expected to be more modulated during the rf cycle.

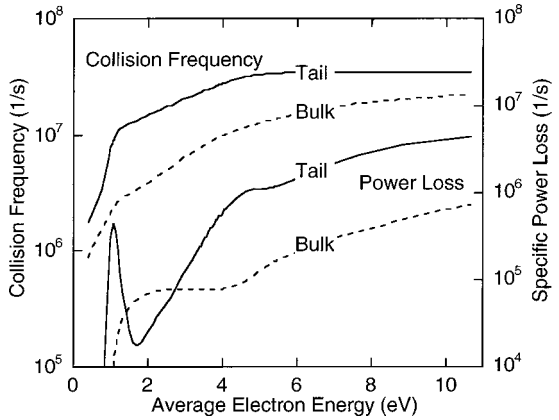

FIG. 2. Collision frequency and specific power loss rate as a function of average electron energy for an $Ar/N_2=80/20$ mixture at 5 mTorr. The tail of the EED is typically more collisional than the bulk for both momentum transfer and power loss.

As a point of departure, the time dependence (as depicted by sequential phases ϕ during the rf cycle) of the source functions for ionization of Ar when including four

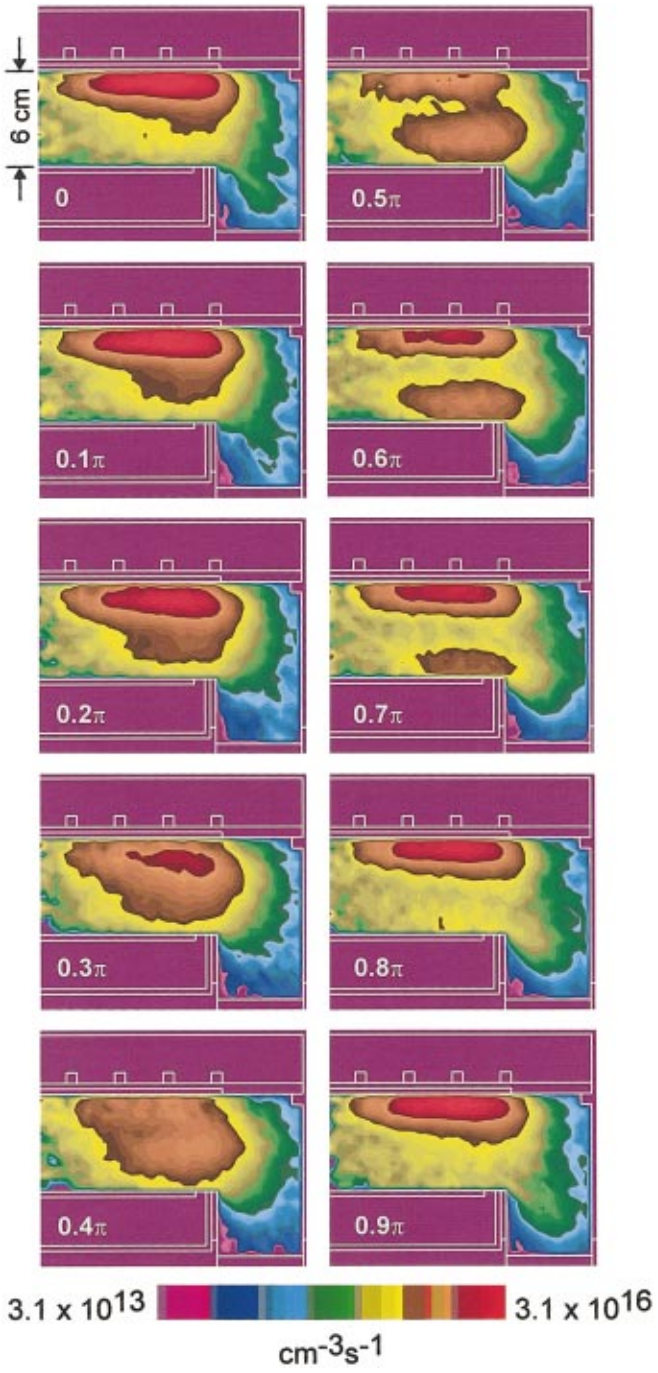

FIG. 3. (Color) Source functions for electron-impact ionization of argon for the base case conditions ($Ar/N_2=90/10$, 5 mTorr, 650 W, 13.56 MHz) for different times during the rf cycle, as indicated by the phase notation in each figure. As even harmonics dominate, results are shown only for the first half of the cycle. Ionization rates are significantly modulated with nonlocal behavior demonstrated by pulses which propagate across the reactor.

harmonics for the base case conditions are shown in Fig. 3 as obtained with the OTF method. Note that only the first half of the cycle is shown as, discussed below, the even harmonics dominate. (For this figure and the results which follow, a phase of zero corresponds to when the electric field adjacent to the dielectric and the antenna current cross zero.) The total electron-impact source functions shown here are the sum of the time-averaged value (the zeroth harmonic) and the harmonic amplitudes multiplied by their corresponding phases.

TABLE I. Ratio of amplitude of harmonics S_n to time averaged amplitude S_0.

	S_n/S_0	
Harmonic	Ar ionization	N_2 $(v=1)$ excitation
1	0.019	0.007
2	0.222	0.041
3	0.017	0.005
4	0.049	0.008

The ratios of the magnitude of the spatially averaged harmonic amplitudes compared to the time-averaged values, S_n/S_0 are shown in Table I. The source function for Ar^+ is near its maximum value, located under the coils, between the phases $\phi=0$ and $\pi/10$. The source function in this volume is heavily modulated, reaching its minimum value approximately $\pi/2$ later in phase. The volume averaged S_n/S_0 for the second and fourth harmonics are 0.22 and 0.05, respectively, compared to 0.02 for the first and third harmonics. The location and periodicity of this excitation would imply that the harmonic heating has a large collisional component due to the twice a period peak in the magnitude of E_θ. There is substantial evidence for noncollisional or long-mean-free-path transport. For example, note the local extrema in the ionization source function which propagates axially across the reactor, resulting from electrons having been accelerated from a volume in the skin depth. This propagating excitation likely results from electrons accelerated by NLF and retaining their energy through noncollisional transport across the reactor.

The amplitudes of the Fourier components as a function of position for the Ar^+ source function are shown in Fig. 4. The electromagnetic skin depth is approximately 2 cm for these conditions. The amplitude of the zeroth component is the time-averaged source function shown in Fig. 1(d). Its maximum is located under the coils where the inductively coupled electric field is largest and decreases at larger radii due to a falloff in electron density, the transport of high-energy electrons from the smaller volume of the electromagnetic skin depth to the larger volume of the periphery of the reactor and to the depletion of NLF accelerated electrons. The source function is most highly modulated near its maximum and in the path of the axial excitation pulse as it propagates across the reactor. In these regions $S_2/S_0 \approx 0.5$. The first and third harmonics should, in principle, be negligible given the 2ω content of the acceleration by the inductively coupled electric field and NLF. We do see, however, spatially diverse, though somewhat numerically noisy, amplitudes for the first and third components, with maxima directly under the coils. These amplitudes, as well as much of the fourth harmonic, result from the nonlinear dependence of excitation rates on excursions of the tail of the EED which in turn generate Fourier components, as discussed below. For this reason alone, the amplitude of the odd components should scale with ν_m/ω. The peak amplitude of the second harmonic, being more than half that of the time-averaged value, signifies that the tail of the EED is highly modulated in the electromagnetic skin depth, a consequence of both collisional processes, and noncollisional transport and NLF heat-

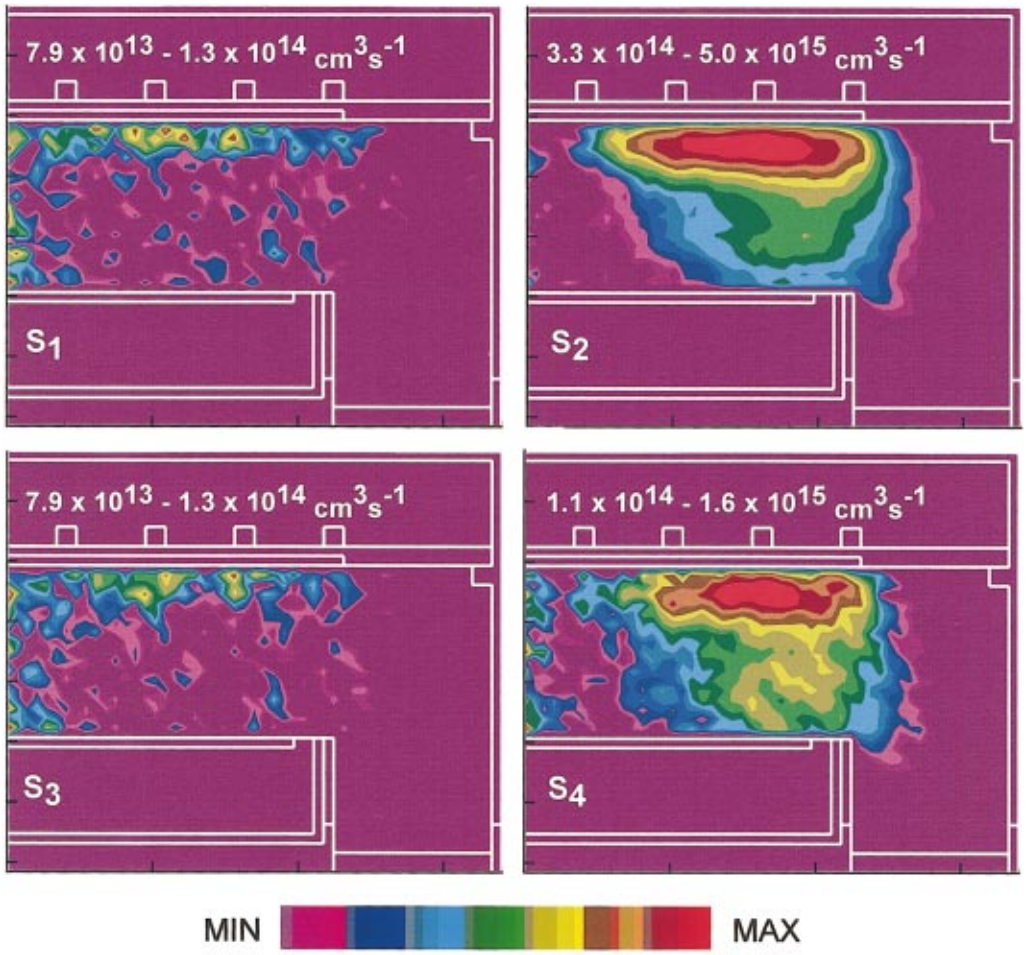

FIG. 4. (Color) Amplitudes of the spatially dependent Fourier coefficients, S_n for harmonic n, for ionization of argon for the base case conditions ($Ar/N_2=90/10$, 5 mTorr, 650 W, 13.56 MHz). The even harmonics dominate, having amplitudes approximately 20% that of the time-averaged value, S_0.

ing which accelerate (or ''launch'') electrons out of the skin depth. The peak amplitude of the fourth component, is approximately 0.15 that of the zeroth, and occurs deeper in the skin depth where the electric field is largest. Another possible contribution to the fourth harmonic is backscattered electrons which, having been initially accelerated forward by the advancing electric field, are back scattered and accelerated a second time during the same half cycle.

Significant harmonic content in ionization rates of Ar was also observed by Oh and Makabe in their particle-in-cell simulations of a 5 cm diameter, cylindrically symmetric, solenoidally driven ICP.[10] At a pressure of 300 mTorr and frequency of 6.78 MHz, the ionization rate was 100% modulated in time at the second harmonic. At 27.12 MHz, the modulation was still significant whereas at 100 MHz, little modulation was observed.

The source functions for vibrational excitation of $N_2(v=1)$ are shown in Fig. 5 as a function of position for different phases during the rf cycle. There is significantly less modulation in both space and time for this low-threshold process compared to the higher-threshold ionization process. The volume averaged fractional harmonic content, S_n/S_0 are 0.041 and 0.008 for the more dominant second and fourth harmonics, and less than 0.007 for the first and third harmonics. This lower degree of modulation reflects the fact that vibrational excitation, with its 0.29 eV threshold, largely responds to the modulation in the bulk portion of the EED. Due to the lower degree of collisionality of these electrons compared to the tail, they retain their energy for larger fractions of the rf cycle after acceleration, and so produce a larger dc component of the excitation rates.

To further illustrate the noncollisional nature of the NLF heating which launches energetic electrons to locations deeper than the electromagnetic skin depth, simulations were performed for a plasma reactor with a taller plasma region while keeping other conditions the same as the base case. The time dependence of the ionization source functions for this reactor are shown in Fig. 6. The amplitude of E_θ is shown in Fig. 7. The field is absorbed and decays to negligible values (<10 mV/cm) 3–4 cm above the substrate. The ionization source function in the skin depth builds throughout the positive half of the cycle and reaches its peak approximately at the zero crossing which implies some substantial contribution from noncollisional heating. The pulse of excitation which propagates across the reactor appears to originate close to the peak in the rf cycle. The ionization pulse propagates at approximately 3.6×10^8 cm/s, corresponding to an electron energy of 35–40 eV. The pulse propagates across the reactor until these energetic electrons

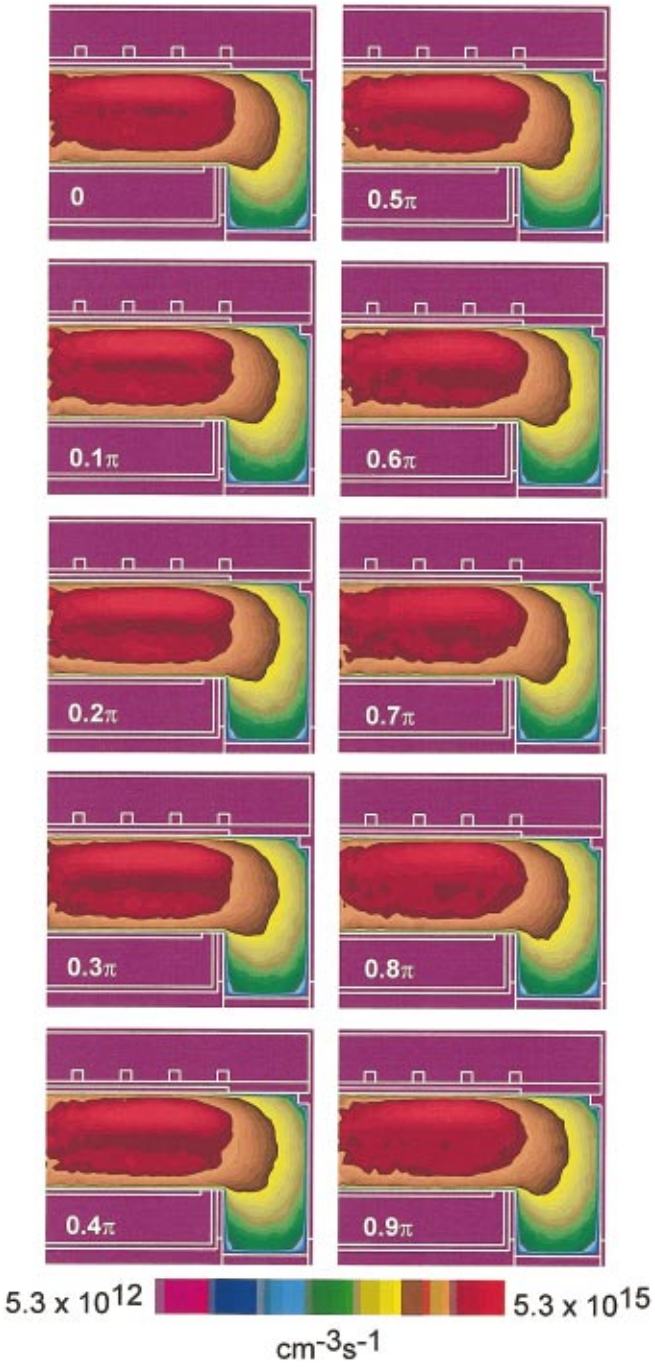

FIG. 5. (Color) Source functions for vibrational excitation of $N_2(v=1)$ of for the base case conditions ($Ar/N_2=90/10$, 5 mTorr, 650 W, 13.56 MHz) for different times during the rf cycle, as indicated by the phase notation in each figure. As even harmonics dominate, results are shown only for the first half of the cycle. There is little modulation of this low threshold energy process.

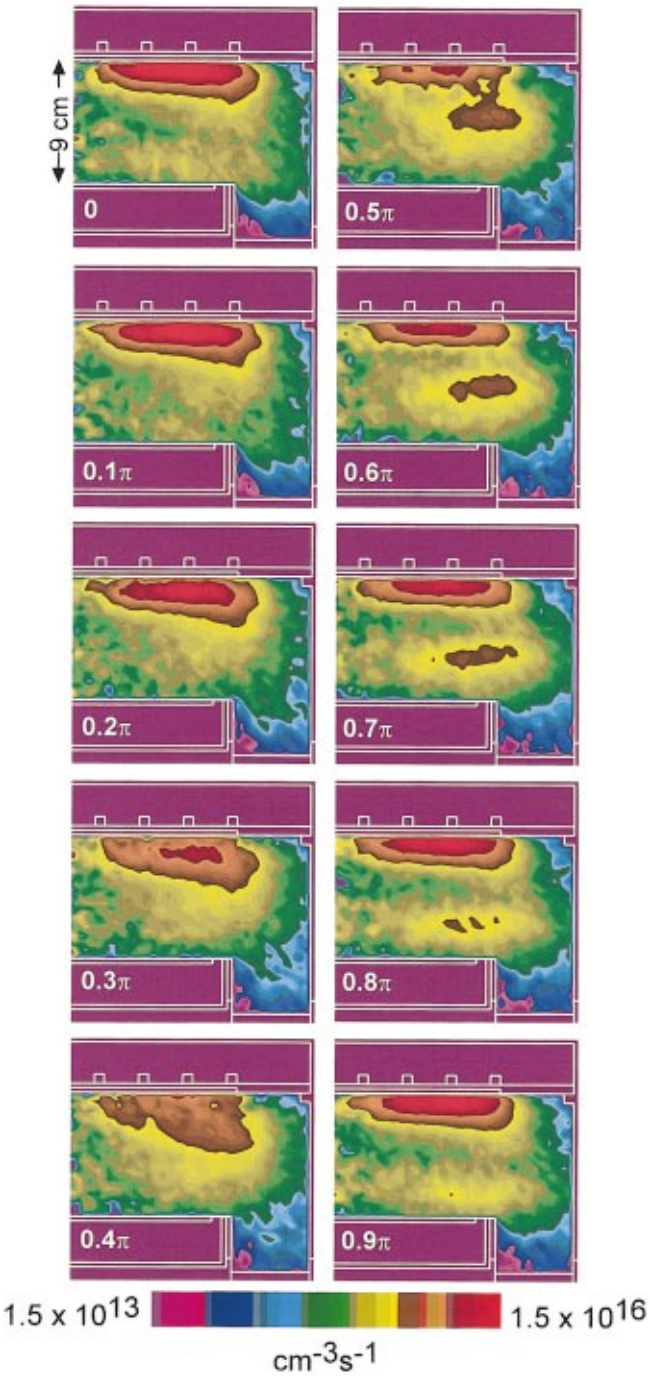

FIG. 6. (Color) Source functions for electron-impact ionization of argon for the conditions of Fig. 3 in a reactor with an extended height. Propagation of the excitation pulse occurs beyond the electromagnetic skin depth, thereby demonstrating noncollisional transport.

impact onto the substrate, crossing regions where the electric field is essentially zero (see Fig. 7).

The temporal dynamics of the ionization source function are significantly different when the rf magnetic field is omitted from the electron acceleration terms, as shown in Fig. 8 for what would otherwise be the base case conditions. The ionization source functions with the rf magnetic field (Fig. 3) and without the rf magnetic field (Fig. 8) both have substantial ionization beyond the electromagnetic skin depth. However the case without the rf magnetic field has less modulation both in the electromagnetic skin depth and beyond, and lacks the distinct ''ballistic'' ionization component which propagates across the reactor as seen for the case with the rf magnetic field. We therefore attribute the ballistic component of the ionization source to the $\vec{v}\times\vec{B}$ acceleration resulting from the rf magnetic field.

In the plasma volume directly under the coil, the azimuthal component of the inductively coupled electric field, E_θ, is roughly parallel to the coils (see Fig. 7). Although the

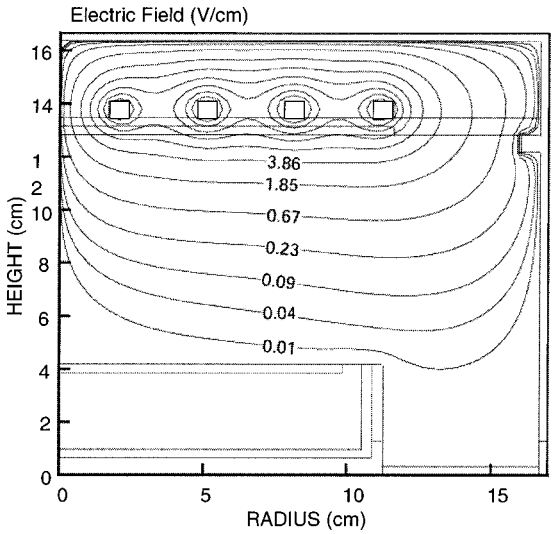

FIG. 7. Amplitude of the inductively coupled electric field for the base case conditions in the extended reactor. The electric field is only 10s mV/cm in the vicinity of the substrate.

rf magnetic field has both radial and axial components, directly under the coils within a few centimeters of the dielectric the rf magnetic field, $B_r=(1/\omega)(\partial E_\theta/\partial z)$, consists dominantly of the radial component which also has contours roughly parallel to the coils. If we approximate $\partial E_\theta/\partial z \approx E_\theta/\delta$, where $\delta=[m_e/(e^2\mu_0 n_e)]^{1/2}$ is the conventional electromagnetic skin depth, then the axial acceleration due to the $\vec{v}\times\vec{B}$ force is approximately $a_z\approx qE_\theta\nu_\theta/\omega\delta$, where v_θ is the net azimuthal component of the electron velocity. At sufficiently low pressure, there is the expectation that the electron energy distribution will have some anisotropy with net velocity in the azimuthal direction. For example, during execution of the electron MCS we calculated the average value of v_θ/v for in the first 1–2 cm of the skin depth for the base case conditions and found $v_\theta/v\approx 0.25$. This value produces a ratio of the axial to azimuthal acceleration of $a_z/a_\theta=F_L/F_E\approx v_\theta/\omega\delta\approx 5n_e^{1/2}\varepsilon^{1/2}/f$ for antenna frequency f where the electron density in the electromagnetic skin depth has units cm^{-3} and the average electron energy has units of eV. For base case conditions ($n_e=10^{11}\ \mathrm{cm}^{-3}, \varepsilon=3\ \mathrm{eV}, f=13.56\ \mathrm{MHz}$), $F_L/F_\theta\approx 0.2-0.25$, which qualitatively agrees with the measurements by Godyak.[17]

The collisional component of heating will be largest when the EED is equilibrated with the inductively coupled electric field. There is the expectation that the rate of equilibration with the electric field will scale with the ratio of the electron energy relaxation collision frequency to the rf frequency. For collision frequencies which are large compared to the rf frequencies (high pressure, small ω), electrons may come into equilibrium with the rf electric field, and so produce high-harmonic content. For large rf frequencies, electrons average over rf periods, thereby responding to only the time-averaged field, and so we should expect low-harmonic content. On the other hand, NLF maximizes at both low frequency (large B_{rf}) and low pressure (small ν_m) producing a large v_θ.

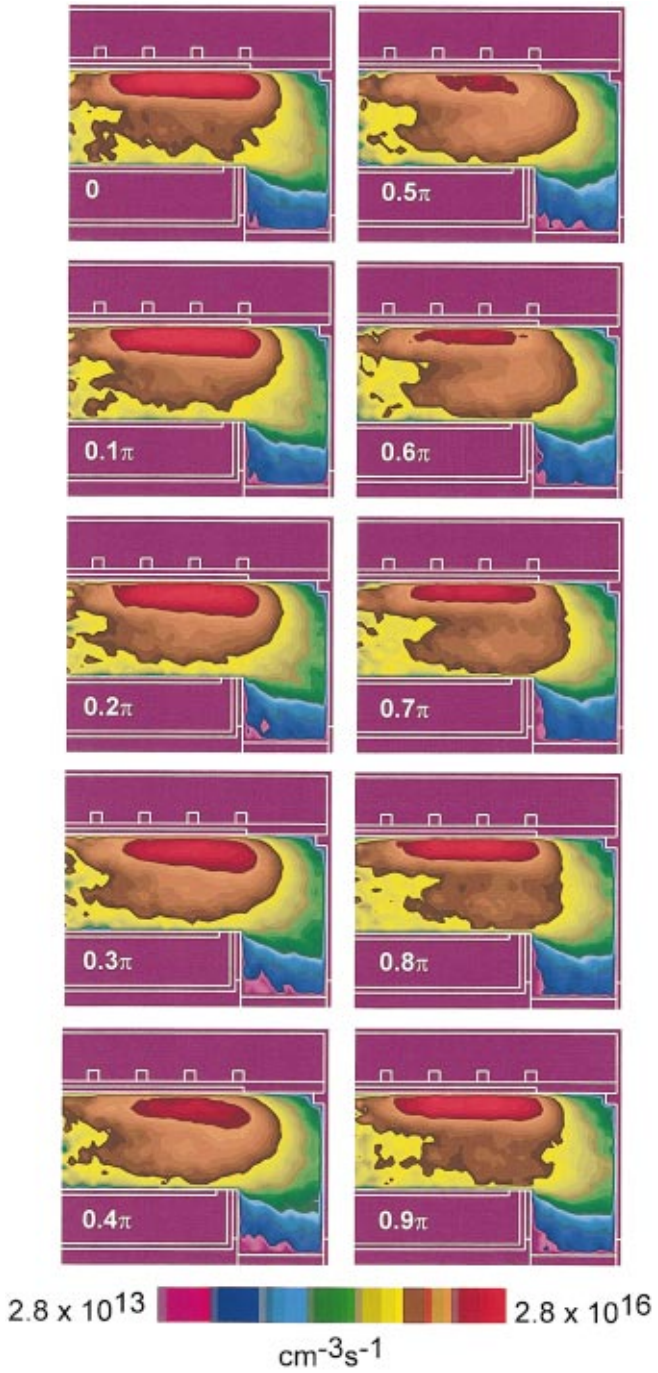

FIG. 8. (Color) Source functions for electron-impact ionization of argon for the base case conditions ($\mathrm{Ar/N_2}=90/10$, 5 mTorr, 650 W, 13.56 MHz) at different times during a rf cycle when excluding the $\vec{\nu}\times\vec{B}$ forces resulting from the rf magnetic field. The propagation of the ionization pulse is less pronounced.

Even for conditions where nonlocal transport is not important and heating is largely collisional, the harmonic content may not simply scale with ν_m/ω, particularly at large values of ν_m/ω due to the nonlinear dependence of excitation rates on E/N. Consider the situation where $\nu_m/\omega \gg 1$ where there is the expectation that the local-field-approximation (LFA) would be valid. Electron-impact rate coefficients for high-threshold events typically depend exponentially on E/N. Therefore, a transition to LFA behavior at

large ν_m/ω will retain a large second harmonic content but also necessitates growth in higher harmonics to reconstruct this exponential dependence.

To demonstrate this sensitivity of the harmonic content of high-threshold events to increasing ν_m/ω compared to T_e, the following procedure was followed. The zero-dimensional electron energy equation was integrated for an $Ar/N_2=80/20$ mixture over a sufficiently large number of rf cycles to achieve a quasisteady state. A Fourier transform was performed of the time dependence of T_e and the rate coefficient for ionization of argon, k_{ion}, over the last few cycles. The ratio S_n/S_0 for harmonics$\leqslant 10$ were then compared. The energy equation we solved was

$$\frac{d\left(\frac{3}{2}n_e k_b T_e\right)}{dt} = \frac{q^2 n_e [E\sin(\omega t)]^2}{m_e \nu_m(T_e)} - \frac{3}{2}n_e k_b \sum_i \frac{2m_e}{M_i} N_i k_m (T_e - T_i) - n_e \sum_{i,j} N_i k_{ij} \varepsilon_{ij}, \tag{12}$$

where k_b is Boltzmann's constant, k_m is the rate coefficient for momentum transfer for species i having density N_i, and mass M_i, and k_{ij} is the rate coefficient for inelastic collision j for species i having energy loss ε_{ij}. The electric field was oscillated at $\omega=10$ MHz having an E/N amplitude of 500 Td (1 Td$=10^{-17}$ V$-$cm^2). Rate coefficients were obtained by solving Boltzmann's equation for the EED using a two-term spherical harmonic expansion over a large range of E/N. A lookup table for the rate coefficients using T_e as the free parameter was then created from the results. This procedure and the immediately following discussion is intended to demonstrate scaling laws and not intended to map directly to the ICPs of interest. The choice of 500 Td corresponds to a few V/cm at 5–20 mTorr, a typical E/N in the skin depth.

Values of S_n/S_0 for T_e and k_{ion} for pressures of 5 and 100 mTorr obtained from analysis of Eq. (12) are shown in Fig. 9. At 5 mTorr, there is significant harmonic content only for the second harmonic reflecting the low value of ν_m/ω (about 0.3 for the bulk and 3 for the tail of the EED) which results in the EED averaging the electric field over the rf cycle.[26] In general, the harmonic content of both T_e and k_{ion} track each other. At 100 mTorr, both T_e and, k_{ion} have significantly more harmonic content, dominantly at the even harmonics (ν_m/ω is about 6 for the bulk and 60 for the tail of the EED). In all even harmonics, S_n/S_0 for k_{ion} is larger (by more than an order of magnitude at higher harmonics) that for T_e. S_n/S_0 for k_{ion} retain these large values through the 20th harmonic. As k_{ion} has an exponential dependence on the electron temperature, small harmonic excursions of T_e are amplified in a highly nonlinear fashion, requiring significant Fourier coefficients extending to high harmonics to reconstruct its time dependence.

Reactor averaged harmonic content of the Ar^+ source function obtained with the OTF method as a function of rf frequency is shown in Fig. 10 where we have retained four harmonics in the analysis. The individual harmonic amplitudes are shown in Fig. 10(a) and the sum of the harmonic amplitudes, ignoring the contributions of phase factors, is shown in Fig. 10(b). The operating conditions are 5 mTorr of $Ar/N_2=90/10$ and a power deposition of 650 W. Increasing frequency decreases both ν_m/ω and $1/(\nu_m\omega)$, and so one should expect lower harmonic content for both collisional and NLF processes. For example, at a frequency of 10 MHz, $\nu_m/\omega\approx 0.15$, which is sufficient for significant amplitudes for the second and fourth harmonics from collisional processes. The individual amplitudes of the harmonics decrease to less than 3% of the time-averaged value at around 30 MHz. In this regime, $\nu_m/\omega\approx 0.05$ which is sufficiently small that electrons respond to the time-averaged field. NLF decreases with increasing ω due to the reduction in B_{rf} and so large harmonic content is not expected from these processes at high frequency. The increase in harmonic content at low ω likely contains contributions from both collisional (linear) and NLF processes.

The harmonic content of the ionization source function as obtained with the OTF method as a function of pressure is shown in Fig. 11 for 13.56 MHz, $Ar/N_2=90/10$, and a power deposition of 650 W. The individual harmonic amplitudes are shown in Fig. 11(a) and their sum is shown in Fig. 11(b).

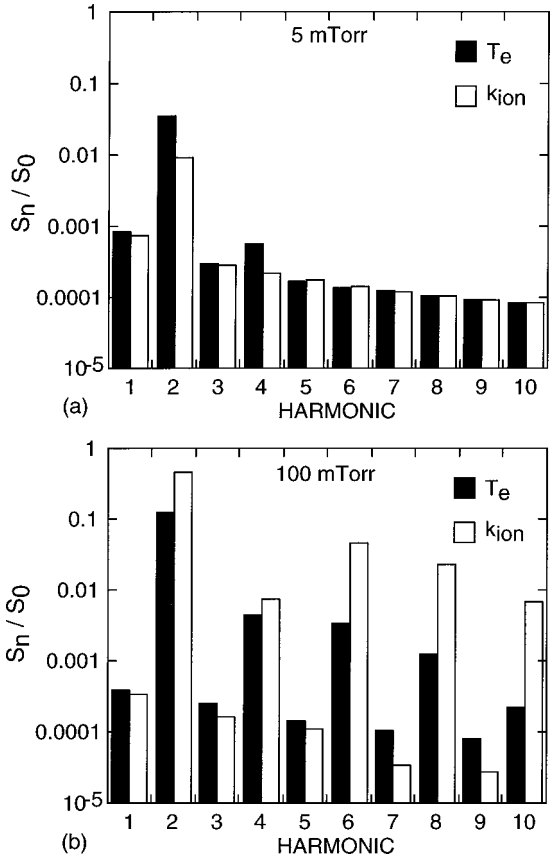

FIG. 9. The ratio of the harmonic amplitudes to the time-averaged value, S_n/S_0, for electron temperature and ionization of argon in an $Ar/N_2=90/10$ gas mixture at 10 MHz obtained by integrating the zero-dimensional electron energy equation. (a) 5 mTorr and (b) 100 mTorr. The harmonic content of both T_e and k_{ion} increase with increasing pressure. Although T_e and k_{ion} have similar harmonic content at the lower pressure, the harmonic content for k_{ion} greatly exceeds T_e at the higher pressure.

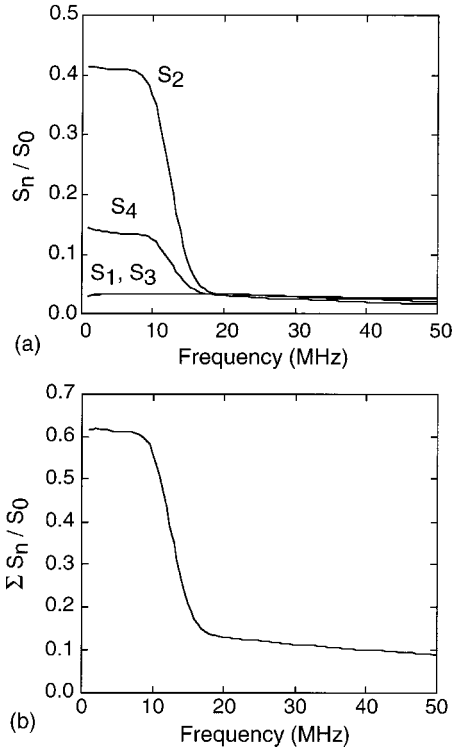

FIG. 10. The ratio of the harmonic amplitudes to the time-averaged value, S_2/S_0, for ionization of argon for the base case conditions except for varying frequency. (a) Individual harmonics and (b) sum of the harmonic amplitudes (ignoring phase factors).

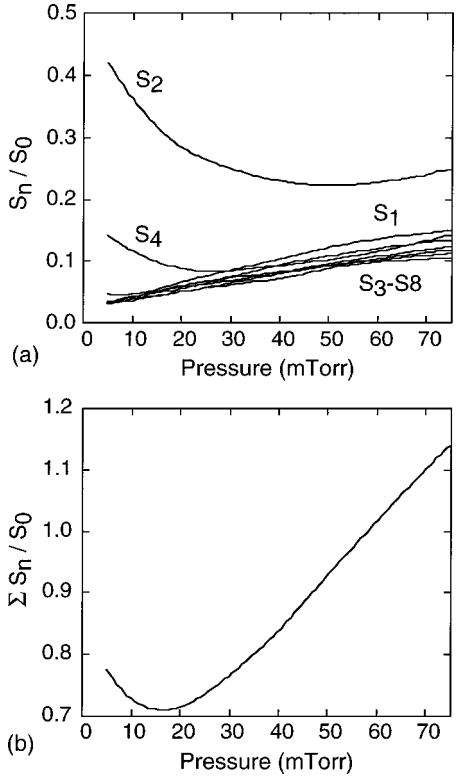

FIG. 11. The ratio of the harmonic amplitudes to the time-averaged value, S_2/S_0, for ionization of argon for the base case conditions except for varying pressure. (a) Individual harmonics and (b) sum of the harmonic amplitudes (ignoring phase factors).

(The sum of the harmonics may be greater than one due to the neglect of phase factors.) For these results, we computed Fourier coefficients through the eight harmonic. Based on only collisional (linear) arguments which use ν_m/ω as a scaling parameter (which scales with pressure), one should expect a monotonic increase in harmonic content when increasing pressure. This trend is seen at pressures greater that 15 mTorr. At lower pressures, there is also a net increase in harmonic content, which is counter intuitive based on collisional arguments. However, at lower pressures, the electron mean free path increases and collision frequency decreases, thereby increasing the magnitude of second-harmonic NLF acceleration. We can attribute the increase in harmonic content at low pressures to this effect.

The effect of gas composition on harmonic content of the source functions was also investigated. To this end, the HPEM-OTF was used to perform parametrizations as a function of frequency were performed for an $Ar/N_2=60/40$ gas mixture and the results are shown in Fig. 12. The harmonic content varied with frequency similarly to the $Ar/N_2=90/10$ gas mixture, decreasing with decreasing values of υ_m/ω. As the collision frequency for $Ar/N_2=60/40$ gas mixtures is about 50% larger than the leaner gas mixture, higher harmonics have significant amplitude to approximately 25 MHz, compared to about 18 MHz for the leaner mixture.

The contributions to the second-harmonic component of excitation between linear processes and NLF was quantified in the following manner. Parametrizations of the HPEM-OTF were performed over a pressure range of 1–10 mTorr and frequency range of 2–10 MHz. Reactor averaged values

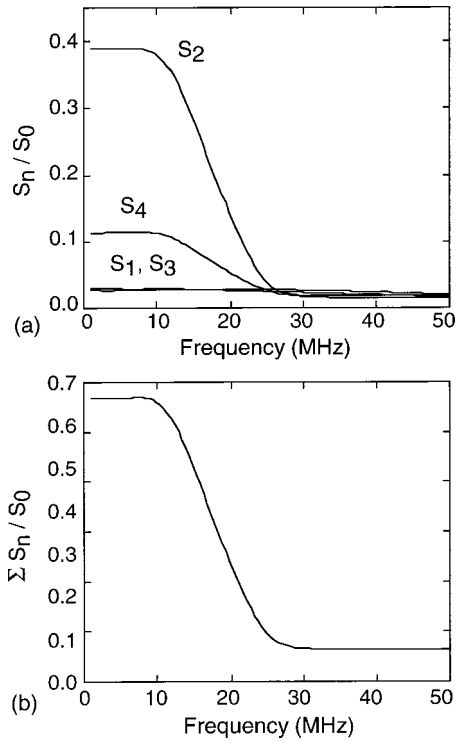

FIG. 12. The ratio of the harmonic amplitudes to the time-averaged value, S_2/S_0, for ionization of argon as a function of frequency for $Ar/N_2=60/40$ at 5 mTorr and 650 W. (a) Individual harmonics and (b) sum of the harmonic amplitudes (ignoring phase factors).

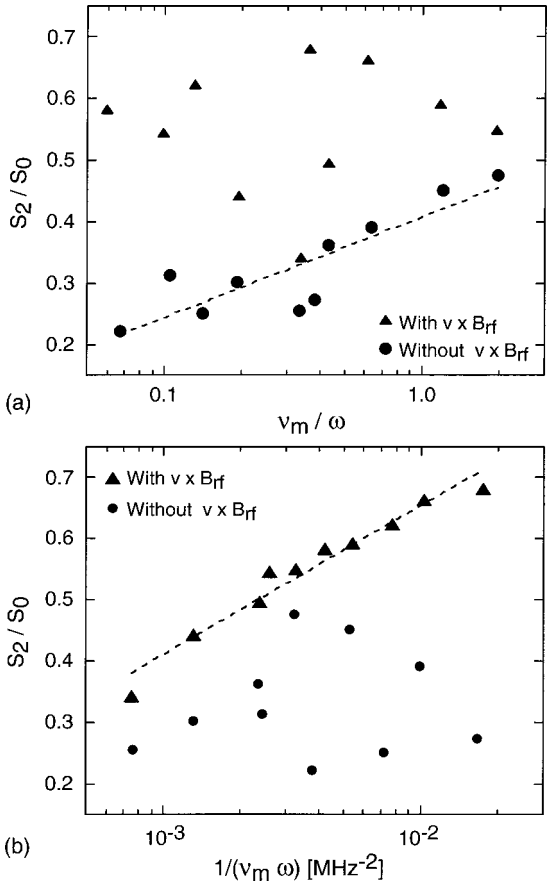

FIG. 13. Reactor averaged S_2/S_0 for ionization of argon in $Ar/N_2=60/40$ gas mixtures for arbitrary combinations of pressure (1–10 mTorr) and rf frequency (2–10 MHz) as a function of (a) ν_m/ω and (b) $1/(\nu_m\omega)$. Results are shown when including and excluding $\vec{v}\times\vec{B}$ terms in the electron acceleration. The dashed lines are logarithmic fits to the data without $\vec{v}\times\vec{B}$ in (a) and with $\vec{v}\times\vec{B}$ in (b). Harmonic content at high values of $1/(\nu_m\omega)$ is attributable to nonlinear Lorentz forces and at high values of ν_m/ω to collisional processes.

of S_2/S_0 for ionization of argon and the time averaged ν_m for an $Ar/N_2=60/40$ gas mixture were computed. Values were obtained when including and excluding the $\vec{v}\times\vec{B}$ terms in the acceleration for electrons in the MCS. S_2/S_0 was then plotted as a function of ν_m/ω and $1/(\nu_m\omega)$.

S_2/S_0 as a function of ν_m/ω for arbitrary combinations of pressure and frequency is shown in Fig. 13(a). The expectation is that S_2/S_0 should scale with ν_m/ω if collisional processes dominate. In all cases, S_2/S_0 is larger when including the $\vec{v}\times\vec{B}$ terms than when excluding them. When including the $\vec{v}\times\vec{B}$ terms, there appears to be no scaling of S_2/S_0 with ν_m/ω. When excluding the $\vec{v}\times\vec{B}$ terms, S_2/S_0 appears to be well correlated with ν_m/ω for large values of ν_m/ω. The dashed line in Fig. 13(a) is a logarithmic fit of S_2/S_0 when excluding the $\vec{v}\times\vec{B}$ terms. Those points which depart from the fit tend to be at the extremes of either pressure of frequency.

S_2/S_0 as a function of $1/(\nu_m\omega)$ for arbitrary combinations of pressure and frequency [same cases as for Fig. 13(a)] is shown in Fig. 13(b). The expectation is that S_2/S_0 should scale with $1/(\nu_m\omega)$ if NLF processes dominate. When including the $\vec{v}\times\vec{B}$ terms, S_2/S_0 is well correlated with $1/(\nu_m\omega)$. The dashed line in Fig. 13(b) is a logarithmic fit of S_2/S_0 when including the $\vec{v}\times\vec{B}$ terms. Those points which depart from the fit again tend to be at the extremes of either pressure or frequency. When excluding the $\vec{v}\times\vec{B}$ terms, S_2/S_0 appears to have no correlation with $1/(\nu_m\omega)$.

Based on the scalings from Fig. 13, it appears that for the pressure and frequency ranges investigated, even harmonic content of excitation rates is largely attributable to NLF, and an appropriate scaling factor is $1/(\nu_m\omega)$. In the absence of the NLF, even harmonic content scales with ν_m/ω, though the magnitude of that harmonic content is smaller.

IV. CONCLUDING REMARKS

To resolve the harmonic content of excitation rates and source functions in low-pressure plasma sources, a Monte Carlo technique was developed and implemented into a two-dimensional plasma equipment model. In the OTF method, moments of the EED and their harmonics are directly computed during integration of the trajectories of the pseudoparticles. Harmonic content of source functions for Ar/N_2 gas mixtures at $<$10s mTorr powered at $<$10s MHz was investigated. We found that high threshold processes such as ionization have significant even harmonic content indicating modulation of the tail of the EED with the half cycle peaks of the inductively coupled electric field. Lower-threshold processes, such as vibrational excitation of N_2, have significantly less harmonic content due, in part, to the electrons in the bulk of the EED being less collisional. We found evidence for significant noncollisional heating and long mean-free-path transport in the form of pulses of ionization which axially propagate across the reactor. These pulses are attributed to nonlinear Lorentz forces producing $\vec{v}\times\vec{B}$ acceleration resulting from the rf magnetic field. The scaling of harmonic content was, on a reactor averaged basis, well correlated with $1/(\nu_m\omega)$ when including $\vec{v}\times\vec{B}$ acceleration, with more harmonic content occurring with larger values of $1/(\nu_m\omega)$. When excluding the NLF terms, harmonic content scaled with ν_m/ω. When varying only frequency, harmonic content increased with decreasing ω, an effect which could be attributed to both NLF and collisional processes. When changing only pressure, we found increases in harmonic content at both high and low pressures. The increase in harmonics at high pressure is attributed to collisional heating which scales with ν_m/ω. The increase at lower pressures is attributed to increasing NLF heating which scales as $1/(\nu_m\omega)$.

ACKNOWLEDGMENTS

This work was supported by the National Science Foundation (CTS99-74962), Applied Materials, Semiconductor Research Corporation, and Sandia National Laboratories.

[1] J. T. C. Lee, N. Layadi, K. V. Guinn, H. L. Maynard, F. P. Klemens, D. E. Ibbotson, I. Tepermeister, P. O. Egan, and R. A. Richardson, J. Vac. Sci. Technol. A **14**, 2510 (1996).
[2] G. diPeso, V. Vahedi, D. Hewitt, and T. Rognlien, J. Vac. Sci. Technol. A **12**, 1387 (1994).

[3] C. Lee, D. B. Graves, M. A. Lieberman, and D. W. Hess, J. Electrochem. Soc. **141**, 1546 (1994).
[4] J. K. Lee, L. Meng, Y. K. Shin, H. J. Lee, and T. H. Chung, Jpn. J. Appl. Phys. **36**, 5714 (1997).
[5] I. D. Kagnovich, B. N. Ramamruthi, and D. J. Economou, Phys. Rev. E **64**, 036 402 (2001).
[6] E. Meeks, P. Ho, A. Ting, and R. J. Buss, J. Vac. Sci. Technol. A **16**, 2227 (1998).
[7] J. T. Gudmundsson, T. Kimura, and M. A. Lieberman, Plasma Sources Sci. Technol. **8**, 22 (1999).
[8] M. Tadokoro, H. Hirata, N. Nakano, Z. L. Petrovic, and T. Makabe, Phys. Rev. E **57**, 43 (1998).
[9] K. Hou, S. Nakagarni, and T. Makabe, Thin Solid Films **386**, 239 (2001).
[10] J.-S. Oh and T. Makabe, Jpn. J. Appl. Phys. **39**, 1358 (2000).
[11] V. A. Godyak, B. Alexandrovich, and V. I. Kolobov, Phys. Rev. E **64**, 026 406 (2001).
[12] D. B. Graves, J. Appl. Phys. **62**, 88 (1987).
[13] T. J. Sommerer, W. N. G. Hitchon, and J. E. Lawler, Phys. Rev. Lett. **63**, 2361 (1989).
[14] M. Meyyappan and T. R. Govindan, IEEE Trans. Plasma Sci. **PS-19**, 122 (1991).
[15] M. Surendra, D. B. Graves, and I. J. Morey, Appl. Phys. Lett. **56**, 1022 (1990).
[16] Z. L. Pertovic, F. Tochikubo, S. Kakuta, and T. Makabe, J. Appl. Phys. **73**, 2163 (1993).
[17] V. A. Godyak, Bulg. J. Phys. **27**, 13 (2000).
[18] V. A. Godyak, B. Alexandrovich, R. Piejak, and A. Smolyakov, Plasma Sources Sci. Technol. **9**, 541 (2000).
[19] R. H. Cohen and T. D. Rognlien, Plasma Sources Sci. Technol. **5**, 442 (1996).
[20] V. A. Godyak, R. Piejak, B. Alexandrovich, and A. Smolyakov, Plasma Sources Sci. Technol. **10**, 459 (2001).
[21] R. B. Piejak and V. A. Godyak, Appl. Phys. Lett. **76**, 2188 (2000).
[22] R. Kinder and M. J. Kushner, J. Vac. Sci. Technol. A **19**, 76 (2001).
[23] R. Kinder and M. J. Kushner, J. Appl. Phys. **90**, 3699 (2001).
[24] C. K. Birdsall and A. B. Langdon, *Plasma Physics by Computer Simulation* (McGraw-Hill, New York, 1985), Sec. 8-5.
[25] N. A. Krall and A. W. Trivelpiece, *Principles of Plasma Physics* (San Francisco Press, San Francisco, 1986), p. 152.
[26] M. J. Pinheiro, G. Gousset, A. Granier, and C. M. Ferreira, Plasma Sources Sci. Technol. **7**, 524 (1998).